ACS APPLIED MATERIALS & INTERFACES

Research Article

Cite This: ACS Appl. Mater. Interfaces 2018, 10, 8117−8123

www.acsami.org

Photolithography-Based Nanopatterning Using Re-entrant Photoresist Profile

Tong June Kim,[†] Yei Hwan Jung,[†] Huilong Zhang, Kwangeun Kim, Juhwan Lee, and Zhenqiang Ma*

Department of Electrical and Computer Engineering, University of Wisconsin-Madison, Madison, Wisconsin 53706, United States

ABSTRACT: Photolithography based on optical mask is widely used in academic research laboratories due to its low cost, simple mechanism, and ability to pattern in micron-sized features on a wafer-scale area. Because the resolution is bound by diffraction limits of the light source, nanoscale patterning using photolithography requires short-wavelength light source combined with sophisticated optical elements, adding complexity and cost. In this paper, a novel method of subwavelength patterning process using conventional i-line mercury lamp is introduced, without the use of such advanced optical tools. The method utilizes the re-entrant geometry of image reversal photoresist produced from the developing process, where a secondary mask is generated by isotropically depositing a metal layer to cover the re-entrant profile of the photoresist. Removing the photoresist by applying ultrasonic vibrations in acetone bath uniformly cracks the metal layer at the sidewalls of the re-entrant profile, exposing the substrate with a reduced feature size. The width of the initial mask pattern can be reduced by 400 nm in a controlled manner, regardless of the original width choice. As a result, the method is shown to achieve sub-100 nm scale linear patterns compatible for both subsequent deposition process and dry-etching process. Our approach is applicable to various shapes of the patterns and can be used in electronic device fabrication requiring nanoscale lithography patterning, such as the gate fabrication of AlGaN/GaN high-electron-mobility transistor.

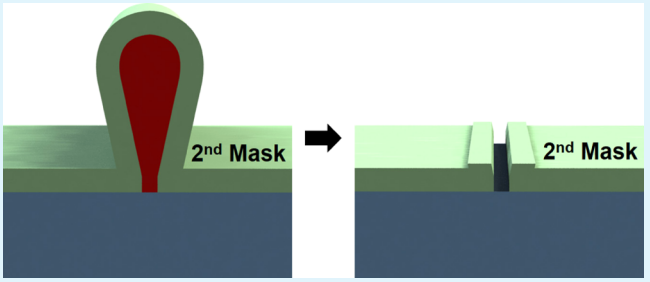

KEYWORDS: *nanopatterning, nanofabrication, subwavelength photolithography, re-entrant profile, high-speed transistor*

1. INTRODUCTION

For many decades, advances in optical lithography have pushed the limits of patterning resolutions and critical length scales of electronic devices from over 15 μm down to sub-10 nm.[1] Such downscaling efforts have made significant enhancements for diverse applications particularly in electronic chips, including the integration density of devices in semiconductor chips and the high-frequency responses in radio frequency (RF) electronics. Because optical lithography is intimately limited by the wavelength of light used, techniques to utilize short wavelengths, such as KrF (248 nm) laser, ArF (198 nm) laser, or even soft X-rays, also known as extreme ultraviolet, have been developed for smaller patterning scales.[2−4] In addition, resolution enhancement techniques that involve multiple optical elements in conjunction with the above-mentioned optical light sources have further reduced the patterning scales.[5,6] However, the high cost of such short-wavelength light sources and optical elements presents challenges in product cost management and in the research and development phase.[7] Consequently, these advanced tools are rarely used in academic laboratories or small industries. Other lithography strategies encounter trade-offs among resolution, throughput, processing time, and feature shape. Direct writing methods like electron-beam lithography and scanning probe-based lithography provide high resolution, but their serial scanning process results in a low throughput and small writing field. Interference lithography[8] and nanoimprint lithography[9] can achieve high-resolution patterns with high throughput over large areas but are associated with limitations. Interference lithography is limited to arrays of regular periodic patterns because the patterns are defined by superimposing different beams, whereas nanoimprint lithography faces problems associated with the mechanical imprinting process, such as defects, template wearing, and removal of residual layers at the printed area.[10−12]

Contact photolithography technology that utilizes Hg lamp (365, 405, and 436 nm) as a light source is commonly used in academic laboratories because of its low cost, wafer-scale productivity, and accessible applicability to diverse micro-fabrication processes. Despite its benefits, the resolution of the patterns is limited due to the diffraction limit of the light source, which creates difficulties in research and development for nanoscale devices.[13] Alternative methods were introduced to pattern subwavelength features by creating resist lens at the surface of the photoresist, while transfer-patterning the metal mask patterns,[14] using near-field photolithography by circumventing the diffraction: coupling and guiding light through elastomeric polymers masks,[15,16] evanescent near-field optical lithography with conformable membrane masks,[17] employing

Received: November 19, 2017
Accepted: January 18, 2018
Published: January 18, 2018

DOI: 10.1021/acsami.7b17628
ACS Appl. Mater. Interfaces 2018, 10, 8117−8123

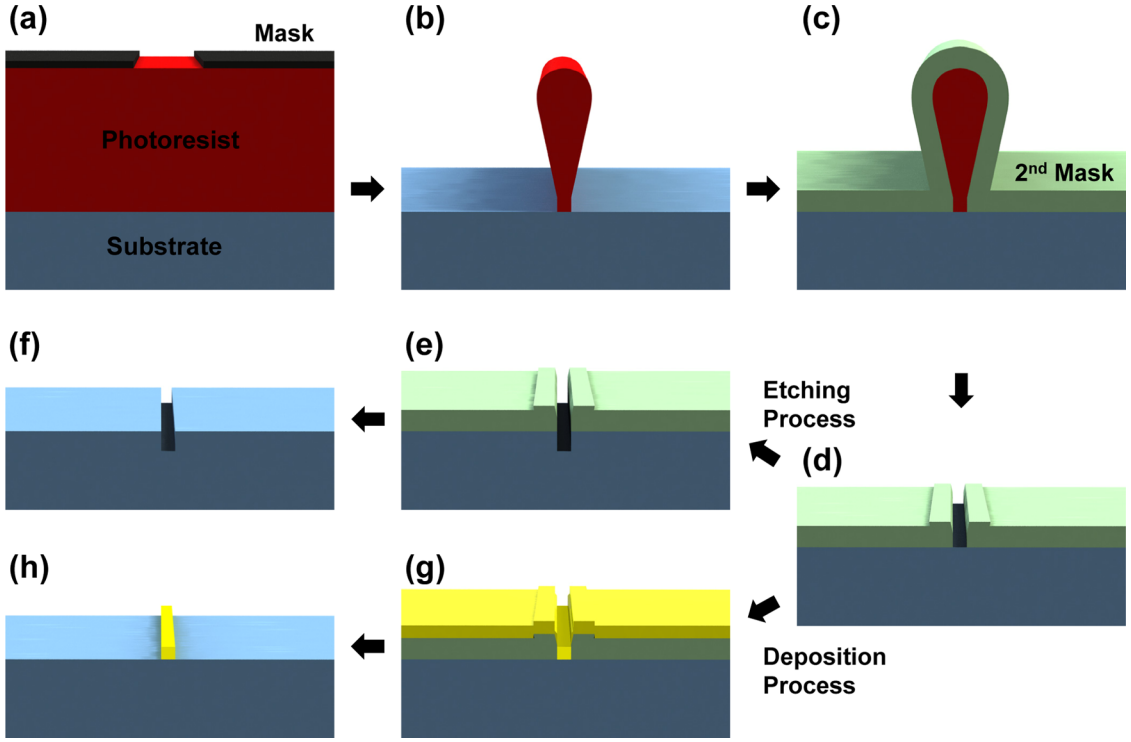

Figure 1. Process flow of subwavelength patterning. (a) Photoresist was spin-coated on the substrate, and the mask patterns were aligned for UV exposure. (b) Photoresist was image-revered and developed for re-entrant profile. (c) A Cr layer was deposited to be utilized for the second mask. (d) Photoresist was removed using ultrasonic vibrations in acetone. (e) Substrate was dry-etched with inductively coupled plasma (ICP)-RIE. (f) The Cr mask layer was removed with Cr etchant. (g) Target metal layers were deposited with e-beam evaporator. (h) The Cr mask layer was used for the lift-off process using Cr etchant. Metal layers on the substrate remains.

surface plasmon polariton with periodic metal masks,[18] and beam pen lithography with metal-coated nanoscale apexes on poly(dimethylsiloxane) masks.[19−21] These techniques, however, require unique mask designs and materials that increase cost and processing time.

In this work, a novel approach to achieve nanoscale lithography patterns using low-cost contact lithography is introduced, which can easily be applied in photolithography processes that are originally designed for microscale patterning. The method utilizes the re-entrant geometry of negative tone or image reversal photoresists produced from contact photolithography tools. In a re-entrant geometry of a layer of photoresist produced using photolithography, the lateral dimension of the top surface is a replica of the photomask used, whereas the dimension of the bottom surface that is in contact with the substrate is undercut etched. The resulting bottom width of the re-entrant photoresist was used as a secondary mask layer by creating a hard mask via isotropic sputtering of metal layer. A subsequent acetone lift-off process with the aid of ultrasonic cleaner was then conducted to remove the photoresist and expose the secondary mask. As a result, a controllable and reproducible sub-100 nm scale patterning was achieved by precisely adjusting the re-entrant profiles, where the critical dimension was successfully reduced from 500 to 70 nm. The practicality of the technique was verified through sub-100 nm dry-etching and metal-deposition processes, two common processes in microfabrication, following the photolithography process. To demonstrate the applicability of the technique, an AlGaN/GaN high-electron-mobility transistor (HEMT) was fabricated with the gate metal deposited using the approach and created a nanoscale gate length, which, in general, improves the high-frequency responses in RF devices.

2. RESULTS AND DISCUSSION

2.1. Subwavelength Patterning Process and Analyzes on the Developing Process. Creating a re-entrant photoresist profile is the key of our process. A negative tone and an image reversal photoresist were originally developed for the clean metal lift-off process of deposited metal films, which was modified for scale reduction patterning. Image reversal photoresist[22,23] utilized in this work is a switchable photoresist that can be modified from a positive tone to a negative tone to create the re-entrant profiles upon development. The switching process is possible because the image reversal photoresist consists of the cross-linking agent that can be activated by UV exposure and baking. The activated area loses the UV light sensitivity and becomes insoluble in the developer, whereas the inactivated area still acts as a positive-tone photoresist under the baking process. After the flood-exposure process, followed by the developing process, only the cross-linked area remains, which means the photoresists acts as a negative tone. Additional advantage of the image reversal photoresist is that edge beads from the spin-coating process can be chemically removed in advance of the image reversal process, which makes further photolithography process easier and cheaper because the process does not require additional edge bead remover. Then, the desired small feature size, key in our work, can be achieved with flawless contact during the UV light exposure.

The process flow of the subwavelength patterning method is shown in Figure 1. Details of the methods are provided in Section 4. Figure 1a shows the photoresist on the substrate with

DOI: 10.1021/acsami.7b17628
ACS Appl. Mater. Interfaces 2018, 10, 8117−8123

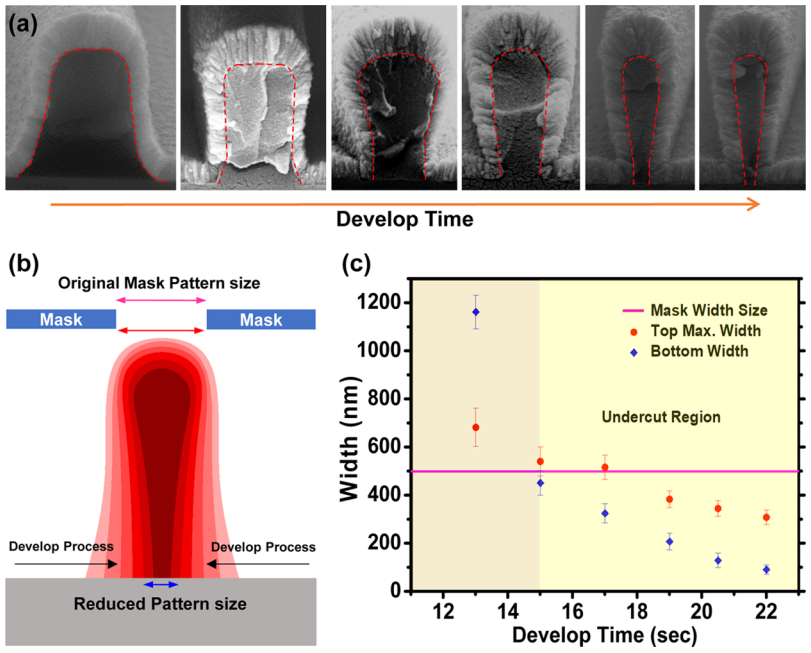

Figure 2. Change in the photoresist profile with respect to developing time. (a) SEM images of the photoresist profile as developing time increased. The red dashed lines indicate the interface between the Cr layer and the photoresist to show the re-entrant profile. (b) Schematic of re-entrant profile change as developing process proceeds. The bottom width of the photoresist developed faster than the upper region of photoresist. (c) The measured width of photoresist with respect to the developing time.

a mask aligned on top to expose the UV light. The resist beads created at the edges of the substrate during the spin-coating process were removed to allow a uniform hard contact between the mask and the photoresist. After the image reversal photolithography process, the cross-sectional geometry of the remaining photoresist profile was a reverse trapezoid because the upper part of the photoresist was cross-linked during the image reversal process to endure the developing process. With additional development time, the top edges of the photoresist rounded, whereas the bottom width was further reduced, resulting in an extreme re-entrant profile, as shown in Figure 1b, due to the developing rate differences. The next step involved deposition of Cr (500 nm) on the substrate using an isotropic deposition tool, such as a sputter. The deposited Cr layer covered all of the surfaces of the sample, including the sidewalls of the photoresist, as shown in Figure 1c. Immersing into acetone and applying ultrasonic vibration uniformly disintegrated the Cr layer on each side of the photoresist strip, exposing the substrate with reduced pattern features achieved from the reduced width of the re-entrant profile (Figure 1d). Compared to the original mask, the size of the new patterns on the Cr layer was reduced significantly. The patterned Cr layer can be used for either dry etching (Figure 1e,f) or deposition (Figure 1g,h). Figure 1e shows the dry-etched substrate using reactive ion etching (RIE), and Figure 1f shows the result of a dry-etched substrate after removing the remains of the Cr layer with Cr etchant. Figure 1g shows the metal layer deposited on the patterned Cr layer using electron-beam evaporator, and Figure 1h shows the remains of the patterned metal after removing the Cr layer with a Cr-selective etchant. Cr was used as the mask layer in this study due to the etchant's high selectivity against other metals, semiconductors, and insulators. Any other material can be substituted if it can be isotropically deposited, depending on the following process and material selectivity.

The most critical process of this method is the developing process of the re-entrant profile (Figure 1a,b). For our experiments, an AZ 5214E (Microchemicals) image reversal resist was applied. Forming the re-entrant profile of the image reversal resist depends on three major controllable parameters. The first parameter is the dose of the UV exposure to cross-link the photoresist. The amount of the exposure needs to be controlled to optimize the re-entrant profile. Over or less dose of the UV light can affect the depth of cross-linking during the image reversal baking, and the profile becomes too steep or shallow. The second parameter is the temperature with enough baking time for activating the cross-linking agents in the photoresist. It must be regulated to obtain the cross-linked area only at the upper region of the photoresist to achieve the re-entrant profile. In this work, the first two parameters were kept in constant and the target profile was studied by varying time of the development process.

Figure 2a shows how the photoresist profile changes with increasing developing time using scanning electron microscopy (SEM) images. SEM images show photoresist profiles deposited with Cr layer using sputter. The developed profiles of the photoresists are indicated in red dashed lines as the developing times are increased from left to right. As the developing time increased, the width of the bottom parts of the photoresist decreased. The profiles are merged and shown in the schematic illustrations in Figure 2b to visualize the decreasing width. The developing rate of the upper region of the photoresist was lower than the photoresist near the substrate because of the intended cross-link of the photoresist near the mask.

Figure 2c shows measurements of the average width of developed profiles with the developing time. The red dots indicate maximum width at the upper region of the resist profile, and the blue dots indicate the width at the bottom region near the substrate. The width of the original mask

DOI: 10.1021/acsami.7b17628
ACS Appl. Mater. Interfaces 2018, 10, 8117−8123

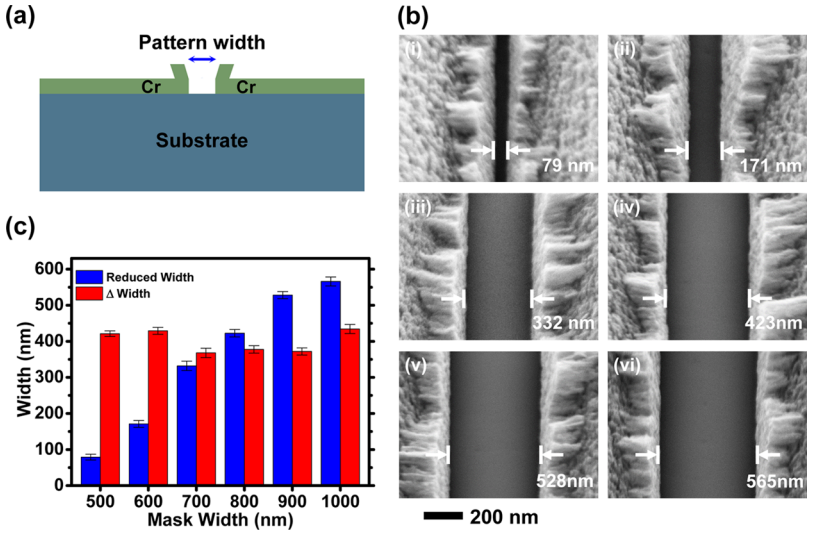

Figure 3. Results of pattern width with different mask feature sizes. (a) Schematic of the second mask layer after removal of the photoresist. (b) SEM images of the exposed substrate with different mask feature sizes. The sizes of the mask features are 500 nm, 600 nm, 700 nm, 800 nm, 900 nm, and 1 μm from (i) to (vi), respectively. (c) Plot of the average actual exposed width of the substrate and the width difference between exposed width and the mask pattern width.

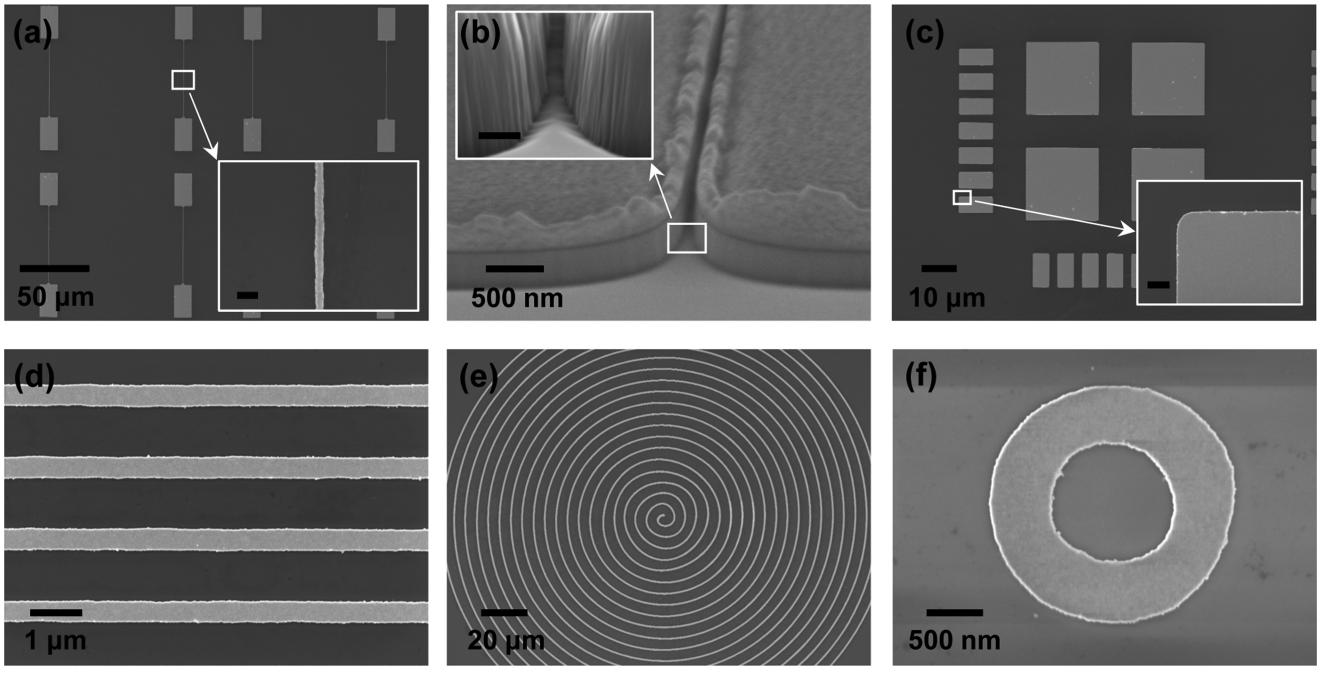

Figure 4. SEM images of various shapes with different processes. (a) Arrays of Ni/Au-deposited sub-100 nm metal strips between two large rectangles (13 μm × 24 μm). The inset shows a magnified area at the metal strip with 70 nm width (scale bar = 200 nm). (b) Dry etching of the substrate using Cr layer as a mask. The inset is the magnified dry-etched trench area. (c) Metal-deposited align marks consist of many rectangle shapes. The inset shows the magnified corner of a rectangle for corner-rounding studies (scale bar = 200 nm). (d) Deposited metal strips. (e) Metal deposited in spiral shape. (f) Metal deposited in donut shape.

pattern was 500 nm, as indicated by the pink line. The two widths (top and bottom) of the patterned photoresist and the mask pattern width were matched in around 15 s of development; the measured widths of both upper and bottom regions were around 500 nm. After 15 s, the developing process started to undercut the photoresist while maintaining the upper region width at 500 nm, a re-entrant profile photolithography process, where the width at the bottom part of the photoresist is shorter than that of the upper region of the photoresist.

The development of the undercut is the key process for subwavelength patterning. With further development, the width at the bottom of the photoresist was narrowed down to 100 nm at 22 s. At the 100 nm range, it is crucial to carefully rinse the developer with deionized (DI) water to prevent the photoresist structures from sagging because the extremely reduced photoresist structures have to support the whole re-entrant photoresist structure. After the rinsing process, a Cr layer was deposited with sputter. To finally expose the nanopattern, the

DOI: 10.1021/acsami.7b17628
ACS Appl. Mater. Interfaces 2018, 10, 8117−8123

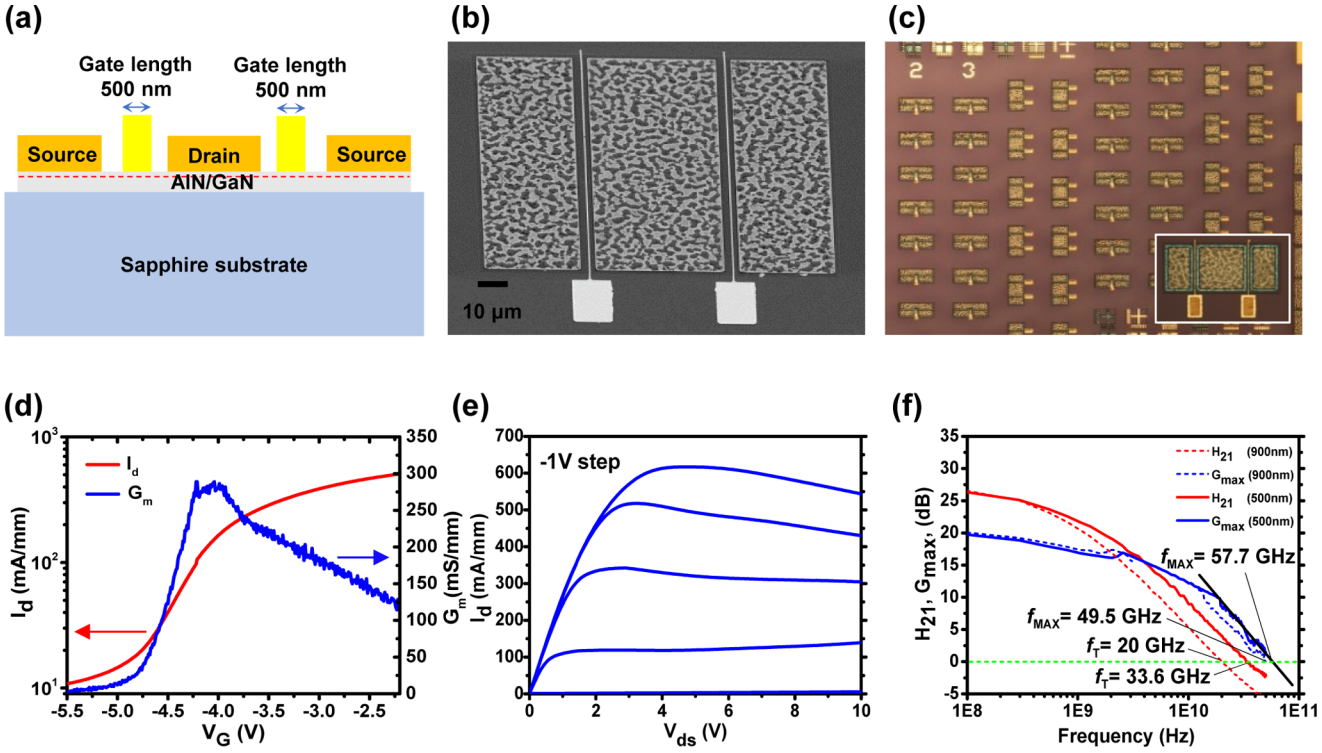

Figure 5. AlGaN/GaN HEMT fabrication with subwavelength photolithography. (a) Schematic of AlGaN/GaN HEMT structure. (b) SEM image of HEMT device after gate metal deposition. (c) Arrays of HEMT devices after via hole opening process. (d) DC performances of an HEMT device. (e) Normalized *I*–*V* characteristics of the HEMT device. (f) Enhancement of RF performances after reducing gate length with subwavelength photolithography technique.

Cr layer at the sidewalls of the photoresist was cracked by applying ultrasonic vibration in acetone, as shown in Figure 3a.

The thickness of the photoresist before processing the re-entrant profile was kept constant, which was around 1.15 μm, by using the same spin-coating recipe. The height of the re-entrant photoresist after developing for 22 s was about 1.05 μm. The thickness of the photoresist was lowered by about 100 nm, whereas the lateral width reduction at the bottom region of the re-entrant profile was about 400 nm from the mask width size. Creating appropriate height of the re-entrant profile is important because the re-entrant photoresist is vulnerable to the force from the sides. The re-entrant photoresist easily collapsed to the side during the rinsing process with DI water or blowing with nitrogen gun after the developing process when the height was too tall. On the other hand, when the thickness of the photoresist was too thin, the formation of re-entrant profile was difficult because the possible height for the undercut decreases.

Further experiments were conducted to test the photoresist's narrowing effect by varying the original mask pattern size. The mask pattern widths varied from 500 nm to 1 μm with an increment of 100 nm, and the resulting photoresist profiles were analyzed in detail, as presented in Figure 3. The patterns were processed and analyzed on a single sample substrate to preserve all other conditions except for the mask pattern size. The SEM images of the exposed area postprocess for different mask widths are shown in Figure 3b (top view) to determine the reduced width. Figure 3b,i–vi shows the patterned results of 500 nm, 600 nm, 700 nm, 800 nm, 900 nm, and 1 μm mask widths, respectively. Figure 3c shows the average reduced widths and changes in widths of the bottom parts of the photoresist with respect to the original mask pattern width. The blue bars represent measured average width of the opened substrate, and the red bars represent the differences between original mask pattern size and average of reduced patterned width. The overall average difference between the original mask width and the reduced width was around 400 nm.

2.2. Postprocess Results and Application to AlGaN/GaN HEMT Fabrication. Figure 4 shows the results of the postdeposition process and post-dry-etching process using the reduced patterns. Figure 4a shows the SEM image of arrays of the deposited patterns with Ni/Au. The Cr layer can be used as a sacrificial layer for the lift-off process when the thickness of the deposited materials is thinner than that of the Cr layer. Ni/Au was deposited using an electron-beam evaporator, which deposits the target material in anisotropic direction. Each deposited pattern has a sub-100 nm strip line in between two large rectangles (13 μm × 24 μm). The strip line at a white box is magnified in the inset and the width was 70 nm. The Cr layer can also be used as a mask for the dry-etching process, and Figure 4b shows the results of the process using inductively coupled plasma-reactive ion etching (ICP-RIE). The remaining Cr layer was left on top of the Si substrate, which can be removed with Cr etchant. The etched trench area indicated in the white box is magnified in the inset, which showed the Si substrate vertically dry-etched with the shape of the Cr layer. Figure 4c is the SEM image of the align marks deposited with Ni/Au during our process. The align marks consisted of many rectangle shapes that gave an opportunity to investigate the corner-rounding phenomenon with our method. The inset is the magnified image at the corner of the rectangle indicated in a white box. The measured corner radius was on average 450 nm. Considering the wavelength of the Hg lamp light source (~400 nm), the corner rounding due to the diffraction of the source

DOI: 10.1021/acsami.7b17628
ACS Appl. Mater. Interfaces 2018, 10, 8117–8123

light is inevitable. An optical proximity correction to the mask pattern[24] is required to enhance the corner-rounding phenomenon.

Some other shapes of the patterns were deposited with our lithography method. Figure 4d shows arrays of metal strips (Ni/Au) deposited on the Si substrate. The width of the strips was 420 nm, separated in 1 μm distances. Figure 4e shows metal line deposition in a spiral shape, and Figure 4f shows the SEM image of a donut-shaped metal deposition. The array of strips and spiral and donut-shaped patterns were processed on the same substrate using a single lithography process. These patterns can be processed in a wafer scale at once, an advantage of the contact photolithography method.

One of the key applications utilizing nanoscale patterns is fabrication of RF electronics. As an example, we demonstrate a high-performance RF device, where the frequency response can be dramatically improved by reducing the gate lengths using the reduction approach.[25] As a way of verifying the feasibility of the patterning process for practical applications, GaN HEMT gate length reduction was demonstrated. A typical method to fabricate gate metal is using e-beam lithography to achieve short gate length, which is often time-consuming and limited to small sample size. Our subwavelength photolithography method replaces the e-beam lithography method, in which an array of HEMT devices were fabricated on a 2.5 mm × 2.5 mm large area. Figure 5a shows a schematic of an HEMT device with double gate fingers. The substrate has an $Al_{0.3}Ga_{0.7}N$/aluminum nitride (AlN)/GaN layer that forms a two-dimensional electron gas for the channel grown on a sapphire wafer. Mesa process was patterned and defined using ICP-RIE. Source and drain metal pads were deposited, followed by annealing in 800 °C for 1 min to make Ohmic contact with the substrate. Gate fingers were deposited using our subwavelength photolithography, and the Cr layer was used for the lift-off process (Figure 5b). After passivating the devices with Al_2O_3 and Si_3N_4, opening of the via holes was processed by RIE. Figure 5c shows an optical image of an HEMT array with the via holes opened. The inset image of Figure 5c shows a magnified HEMT device ready for the RF metal pad deposition. Finally, RF metal pads were deposited to measure the HEMT device. Figures 5d shows direct-current (DC) performances of the 2 μm × 50 μm double gate fingers HEMT device with 4.5 μm drain to source separation. The red line represents the transfer curve, and the blue line represents the transconductance curve, both normalized with the gate width. In measuring the performances, the gate voltage was swept from −5.5 to 0 V while holding the drain to source voltage at 8 V. The maximum transconductance was 289 mS/mm at V_g = −4.04 V, which was the bias point used to measure RF performances. Figure 5e shows the normalized I−V characteristics of the same device. The drain currents were measured by changing the gate voltages from −5 to −1 V with a step size of 1 V, whereas the drain voltage was swept from 0 to 10 V.

Figure 5f shows the RF performances of the devices with the same dimensions except for the gate length. The gate length without reduction was 900 nm and was reduced using our method to 500 nm. The measured unity current-gain frequency (f_T) after a de-embedding process was 20 GHz, and it was improved to 33.6 GHz as the gate length reduced to 500 nm. The maximum oscillation frequency (f_{max}) was also increased from 49.5 to 57.7 GHz. The measured DC and RF performances show typical behavior of GaN HEMT, proving that our lithography method is applicable to electronic devices.[26]

3. CONCLUSIONS

We developed a novel contact photolithography method to improve the resolution of patterning below the wavelength of the source light, which is simple and economic. The method is proven to narrow down the width of patterning to sub-100 nm, and the application of the method showed an average 400 nm reduction for mask patterns sized between 500 nm and 1 μm. Demonstration of the method in patterning various shapes and fabrication of the GaN HEMT device suggest future applicability to various electronic devices at lower cost. Further enhancement of the resolution requires optimization of the re-entrant profile, which depends on photoresist type and the developing process.

4. EXPERIMENTAL SECTION

4.1. Subwavelength Patterning Method. On a temporary Si substrate, a layer of photoresist (AZ 5214E, 1 μm) was spin-cast at 5 500 rpm for 30 s, followed by soft baking at 95 °C for 3 min. The edge beads of the photoresist were exposed to UV light for 1 min with a dose of 17 mW/cm, whereas the other area for the patterning experiments was protected with a mask. The light intensity of a Hg lamp at the mask aligner (MJB3, Karl Suss) was controlled by a power supply (CIC-500, Karl Suss) using feedback from the UV sensor at the aligner, which was calibrated to sense light intensity at a wavelength of 320 nm. After developing with a developer (AZ 917, Microchemicals) for 30 s and rinsing with DI water, the remaining photoresists of the edge beads were swabbed with acetone-soaked Q-tips. The sample was placed on a hot plate at 95 °C for 1 min to vaporize the remaining solvents at the photoresist and the Si substrate. The patterns were transferred on the photoresist by exposing UV light for 6 s after hard-contacting the photoresist to the mask. The patterns were image-reversed by baking on a hot plate at 110 °C for 90 s. After developing the photoresist in re-entrant profile, Cr was deposited using sputter (CVC 601, 500 nm) to make a secondary mask layer. Immersing into acetone and applying ultrasonic vibration removed most of the photoresist strips, and the remaining strips were completely removed by swabbing gently with Q-tips. Other areas without any patterning feature were protected by Cr layer from the Q-tip swabbing. For the Si substrate etching process, ICP-RIE (Plasma-Therm SLR Series, BCl_3 = 20 sccm, Cl_2 = 20 sccm, pressure = 5 mTorr, RF1 power = 200 W, RF2 power = 300 W) was used for 2 min, followed by removal of the Cr layer with Cr etchant (CEP-200, Microchrome Technology). An electron-beam evaporator was used for the deposition process, followed by lift-off of the Cr layer with Cr etchant.

4.2. Fabrication of AlGaN/GaN HEMT. The fabrication began with AlGaN/GaN layers epitaxially grown on double-sided polished sapphire wafer (4 in. diameter, CREE). The epitaxial layers consisted of undoped GaN (5 μm), undoped AlN (1 nm), undoped $Al_{0.3}Ga_{0.7}N$ (20 nm), and undoped GaN layer (2 nm). The GaN substrate was diced into 6 mm × 6 mm squares with a dicing saw. Mesa patterns for an individual HEMT device were defined using photolithography (AZ 5214E), followed by etching 80 nm of the GaN layer with ICP-RIE (Plasma-Therm SLR Series, BCl_3 = 10 sccm, Cl_2 = 16 sccm, Ar = 3 sccm, pressure = 4 mTorr, RF1 power = 100 W, RF2 power = 500 W, recipe). After removing the residual photoresist on the GaN layer, source and drain metal pads were patterned for the lift-off process with photoresist (AZ 5214E). Rinsing with diluted HCl (HCl/DI water = 1:3) for 1 min removed the oxide layer on the GaN surface. Ohmic metal layers (Ti/Al/Ni/Au, 20/100/45/55 nm) were deposited with an electron-beam evaporator via the lift-off process, followed by a rapid thermal annealing (Heatpulse 610, AG Associates) process at 800 °C for 1 min under N_2 ambient condition. Gate metal layers were patterned with the subwavelength patterning method using Cr (500 nm) and deposited with Ni/Au (20/400 nm) layers using an electron-

DOI: 10.1021/acsami.7b17628
ACS Appl. Mater. Interfaces 2018, 10, 8117−8123

beam evaporator. After the lift-off process with Cr etchant, the devices were passivated with Al_2O_3 (20 nm) using atomic layer deposition and Si_3N_4 using plasma-enhanced chemical vapor deposition (Plasma-Therm, 200 nm). Via holes were opened at gate, source, and drain metal pads using RIE, followed by deposition of RF metal pads (Ti/Au, 10/250 nm) using an electron-beam evaporator.

4.3. Measurement and Analysis. DC performances of the HEMT were measured using HP 4155B Semiconductor Parameter Analyzer. An Agilent E8364A PNA Series Network Analyzer was used to measure the S-parameter of the HEMT with the measurement setup calibrated to the Infinity G-S-G probe tips with 150 μm pitch using a standard Short-Open-Load-Thru (SOLT) calibration kit. The *S* parameters obtained from the RF measurements were analyzed using the advanced design system software.

AUTHOR INFORMATION

Corresponding Author

*E-mail: mazq@engr.wisc.edu.

ORCID

Tong June Kim: 0000-0003-3702-9424

Kwangeun Kim: 0000-0001-6942-7481

Zhenqiang Ma: 0000-0001-9214-1342

Author Contributions

†T.J.K. and Y.H.J. contributed equally to this work.

Notes

The authors declare no competing financial interest.

ACKNOWLEDGMENTS

This work was supported by the Air Force Office of Scientific Research (AFOSR): Presidential Early Career Award in Science & Engineering (PECASE) grant # FA9550-09-1-0482. The program manager is Dr. Gernot Pomrenke. Yei Hwan Jung was a Howard Hughes Medical Institute International Student Research Fellow.

REFERENCES

(1) Ito, T.; Okazaki, S. Pushing the limits of lithography. *Nature* **2000**, *406*, 1027−1031.

(2) Sato, T.; Nakase, M.; Nonaka, M.; Higashikawa, I.; Horiike, Y. KrF Excimer Laser Projection Lithography: 0.35 μm Minimum Space VLSI Pattern Fabrication by a Tri-Level Resist Process. *Jpn. J. Appl. Phys., Part 1* **1988**, *27*, 323−327.

(3) Yen, A.; Anderson, E. H.; Ghanbari, R. A.; Schattenburg, M. L.; Smith, H. I. Achromatic Holographic Configuration for 100-nm-Period Lithography. *Appl. Opt.* **1992**, *31*, 4540−4545.

(4) Bjorkholm, J. E.; Bokor, J.; Eichner, L.; Freeman, R. R.; Gregus, J.; Jewell, T. E.; Mansfield, W. M.; Macdowell, A. A.; Raab, E. L.; Silfvast, W. T.; Szeto, L. H.; Tennant, D. M.; Waskiewicz, W. K.; White, D. L.; Windt, D. L.; Wood, O. R.; Bruning, J. H. Reduction Imaging at 14 nm Using Multilayer-Coated Optics - Printing of Features Smaller Than 0.1 μm. *J. Vac. Sci. Technol., B: Microelectron. Nanometer Struct.* **1990**, *8*, 1509−1513.

(5) Levenson, M. D.; Viswanathan, N. S.; Simpson, R. A. Improving Resolution in Photolithography with a Phase-Shifting Mask. *IEEE Trans. Electron Devices* **1982**, *29*, 1828−1836.

(6) Matsuo, S.; Komatsu, K.; Takeuchi, Y.; Tamechika, E.; Mimura, Y.; Harada, K. In *High Resolution Optical Lithography System Using Oblique Incidence Illumination*, International Electron Devices Meeting 1991 [Technical Digest], Dec 8−11, 1991, 1991; pp 970−972.

(7) Levinson, H. J. *Principles of Lithography*; SPIE Press: Bellingham, WA, 2001; pp 317−334.

(8) Solak, H. H.; David, C.; Gobrecht, J.; Golovkina, V.; Cerrina, F.; Kim, S. O.; Nealey, P. F. Sub-50 nm period patterns with EUV interference lithography. *Microelectron. Eng.* **2003**, *67*−*68*, 56−62.

(9) Chou, S. Y.; Krauss, P. R.; Renstrom, P. J. Imprint lithography with 25-nanometer resolution. *Science* **1996**, *272*, 85−87.

(10) Chen, L.; Deng, X. G.; Wang, J.; Takahashi, K.; Liu, F. Defect control in nanoimprint lithography. *J. Vac. Sci. Technol., B: Microelectron. Nanometer Struct.* **2005**, *23*, 2933−2938.

(11) Tucher, N.; Hohn, O.; Hauser, H.; Muller, C.; Blasi, B. Characterizing the degradation of PDMS stamps in nanoimprint lithography. *Microelectron. Eng.* **2017**, *180*, 40−44.

(12) Otto, M.; Bender, M.; Hadam, B.; Spangenberg, B.; Kurz, H. Characterization and application of a UV-based imprint technique. *Microelectron. Eng.* **2001**, *57*−*58*, 361−366.

(13) Madou, M. J. *Fundamentals of Microfabrication and Nanotechnology*, 3rd ed.; CRC Press: Boca Raton, FL, 2012.

(14) Kim, T. I.; Baek, C. H.; Suh, K. Y.; Seo, S. M.; Lee, H. H. Optical lithography with printed metal mask and a simple superhydrophobic surface. *Small* **2008**, *4*, 182−185.

(15) Rogers, J. A.; Paul, K. E.; Jackman, R. J.; Whitesides, G. M. Using an elastomeric phase mask for sub-100 nm photolithography in the optical near field. *Appl. Phys. Lett.* **1997**, *70*, 2658−2660.

(16) Schmid, H.; Biebuyck, H.; Michel, B.; Martin, O. J. F. Light-coupling masks for lensless, sub-wavelength optical lithography. *Appl. Phys. Lett.* **1998**, *72*, 2379−2381.

(17) Alkaisi, M. M.; Blaikie, R. J.; McNab, S. J.; Cheung, R.; Cumming, D. R. S. Sub-diffraction-limited patterning using evanescent near-field optical lithography. *Appl. Phys. Lett.* **1999**, *75*, 3560−3562.

(18) Luo, X. G.; Ishihara, T. Surface plasmon resonant interference nanolithography technique. *Appl. Phys. Lett.* **2004**, *84*, 4780−4782.

(19) Huo, F.; Zheng, G. F.; Liao, X.; Giam, L. R.; Chai, J. A.; Chen, X. D.; Shim, W. Y.; Mirkin, C. A. Beam pen lithography. *Nat. Nanotechnol.* **2010**, *5*, 637−640.

(20) Liao, X.; Brown, K. A.; Schmucker, A. L.; Liu, G. L.; He, S.; Shim, W.; Mirkin, C. A. Desktop nanofabrication with massively multiplexed beam pen lithography. *Nat. Commun.* **2013**, *4*, No. 2103.

(21) Wu, J.; Yu, C. H.; Li, S. Z.; Zou, B. H.; Liu, Y. Y.; Zhu, X. Q.; Guo, Y. Y.; Xu, H. B.; Zhang, W. N.; Zhang, L. P.; Liu, B.; Tian, D. B.; Huang, W.; Sheetz, M. P.; Huo, F. W. Parallel Near-Field Photolithography with Metal-Coated Elastomeric Masks. *Langmuir* **2015**, *31*, 1210−1217.

(22) Ailing, E.; Stauffer, C. Image Reversal of Positive Photoresist - a New Tool for Advancing Integrated-CircuitFabrication. *Proc. SPIE* **1985**, *539*, 194−218.

(23) Klose, H.; Sigush, R.; Arden, W. Image Reversal of Positive Photoresist - Characterization and Modeling. *IEEE Trans. Electron Devices* **1985**, *32*, 1654−1661.

(24) Poonawala, A.; Milanfar, P. Mask design for optical microlithography - An inverse imaging problem. *IEEE Trans. Image Process.* **2007**, *16*, 774−788.

(25) Sze, S. M. *High-Speed Semiconductor Devices*; Wiley: New York, 1990.

(26) Mishra, U. K.; Parikh, P.; Wu, Y. F. AlGaN/GaN HEMTs - An overview of device operation and applications. *Proc. IEEE* **2002**, *90*, 1022−1031.

DOI: 10.1021/acsami.7b17628
ACS Appl. Mater. Interfaces 2018, 10, 8117−8123